PAPER

Check for updates

A non-enzymatic electrochemical sensor based on nitrogen-doped mesoporous carbon@hydroxyl-functionalized ionic liquid composites modified electrode for the detection of fenitrothion†

Xinsheng Liu,[a] Yutong Li,[b] Wenli Qiao,[b] Mengjun Chang[b] and Yonghong Li 🆔 *[bc]

The overuse of organophosphorus pesticides (OPs) results in severe environmental pollution and food safety issues. Fenitrothion (FNT) is a typical derivative of OPs, so rapid and sensitive detection of FNT plays an important role in environmental protection and public health. An FNT non-enzymatic electrochemical sensor based on nitrogen-doped mesoporous carbon@functionalized ionic liquid composites (N-CMK-3@IL) was constructed in this work. The surface topography and electrochemical properties of the sensor were investigated by scanning electron microscopy (SEM), cyclic voltammetry (CV) and electrochemical impedance spectroscopy (EIS), respectively. Because N-CMK-3@IL composites could improve the conductivity and increase the active surface area of the modified electrode, the sensor exhibited good electrocatalytic activity to FNT. Under the optimal experimental conditions, a good linear relationship for FNT was obtained in the range of 0.5–100 ng mL^{-1}, and the detection limit was 0.1 ng mL^{-1} (S/N = 3). The sensor was successfully applied for the detection of FNT in vegetable samples.

1. Introduction

Organophosphorus pesticides (OPs) are widely used in crops to improve their quality and yield. The overuse of OPs can cause various environmental and ecological problems through soil, atmosphere and water.[1] OPs can cause a variety of central nervous system symptoms to humans by inhibiting acetylcholinesterase and accumulating acetylcholine. OPs may result in serious gestational hypertension, teratogenesis, pulmonary edema, and respiratory paralysis.[2] Therefore, the rapid and sensitive detection of organophosphorus pesticides is of great importance for environmental protection and public health.

Various techniques, such as high-performance liquid chromatography (HPLC), gas chromatography coupled to mass spectrometry (GC-MS) and electrochemical methods, have been developed to detect Ops.[3–9] However, the traditional detection methods need expensive equipment and time-consuming sample pretreatment. With the advantages of simplicity, low cost, quick response, and high sensitivity, the electrochemical methods are regarded as promising techniques for the analysis

of OPs.[10–12] The Ops electrochemical sensors contain enzymatic and non-enzymatic sensors in this field. Because enzymes are biological substances, the enzymatic sensors are affected by pH value, temperature, humidity, and toxic chemicals, which can lead to instability, complex storage and transportation. In order to overcome these limitations, non-enzymatic sensors have attracted increasing interest due to their great sensitivity, quick response, good stability and reproducibility. Fenitrothion (FNT) is a typical derivative of OPs, it can be directly analyzed by the electrochemical methods due to the nitro group in its structure. Therefore, it is possible to develop a non-enzymatic electrochemical sensor for the accurate and quick analysis of FNT.

Ordered mesoporous materials with unique properties have been widely studied in the non-enzymatic electrochemical field. Among them, ordered mesoporous carbon owns adjustable pore structure and large specific surface area, exhibiting good electrical properties and chemical stability.[13–15] In addition, ordered mesoporous carbon doped with nitrogen atoms can improve its affinity and provide more electroactive sites.[16] These superior electrochemical properties make it possible to improve the performance of electrochemical sensors. Meanwhile, ionic liquids exhibit high viscosity, good conductivity, as well as wide electrochemical window.[17,18] Apart from the common characteristics of ionic liquids, hydroxyl-functionalized ionic liquids possess strong hydrogen bonds and high surface tension.

In this work, a non-enzymatic FNT electrochemical sensor based on nitrogen-doped mesoporous carbon@hydroxyl-functionalized ionic liquid composites modified glassy carbon

[a]School of Basic Medical Sciences, Ningxia Medical University, Yinchuan 750004, P. R. China. Fax: +86-951-6980139; Tel: +86-951-6980139

[b]School of Public Health, Ningxia Medical University, Yinchuan 750004, P. R. China. E-mail: yonghongli2012@163.com

[c]Key Laboratory of Environmental Factors and Chronic Disease Control, Yinchuan 750004, P. R. China

† Electronic supplementary information (ESI) available. See DOI: https://doi.org/10.1039/d3ra01011b

electrode was firstly prepared by drop-casting method. The surface morphologies and structural characterization of nitrogen-doped mesoporous carbon@hydroxyl-functionalized ionic liquid composites was performed using scanning electron microscopy (SEM) and X-ray photoelectron spectroscopy (XPS). The electrochemical properties of the modified electrodes were studied by cyclic voltammetry (CV) and electrochemical impedance spectroscopy (EIS). The constructed sensor showed good electrocatalytic activity and ultra-sensitive response to FNT. Furthermore, the fabricated sensor was successfully applied to analyze FNT in vegetable samples. The proposed sensor offered the advantages such as simple preparation process, high sensitivity and stability for the determination of FNT.

2. Experimental

2.1. Reagents and materials

Nitrogen-doped mesoporous carbon (N-CMK-3, particle diameter: 1 μm) was acquired from Nanjing XFNANO Materials Technology Co. Ltd. Ionic liquid 1-hydroxyethyl-3-methylimidazolium tetrafluoroborate ([HOEtMlm]BF$_4$) was purchased from Qingdao OLIKE New Material Technology Co. Ltd. Fenitrothion (FNT) was obtained from Sigma-Aldrich Co., Ltd. 0.1 M phosphate buffer (PBS) was prepared with potassium dihydrogen phosphate (KH$_2$PO$_4$) and disodium hydrogen phosphate (Na$_2$HPO$_4$). Ultrapure water used in the experiment was provided by the Heal Force EASY50 water purification system (Shanghai Canrex Analytical Instrument Co., Ltd.).

2.2. Apparatus

The electrochemical measurement (containing electrochemical impedance spectroscopy) was completed on the electrochemical workstation (CHI660E, Shanghai Chenhua Instrument Co., Ltd.)

and PARSTAT 4000 electrochemical workstation (Princeton, USA). The modified glassy carbon electrode as the working electrode, a platinum wire as the auxiliary electrode, and a saturated calomel electrode (3 M KCl) as the reference electrode formed a three-electrode system. The Hitachi S-3400N scanning electron microscope was used to explore the surface morphologies of the modified electrode (Tokyo, Japan). The X-ray photoelectron spectroscopy was obtained with X-ray photoelectron spectrometer (America Thermo Scientific ESCALAB Xi+).
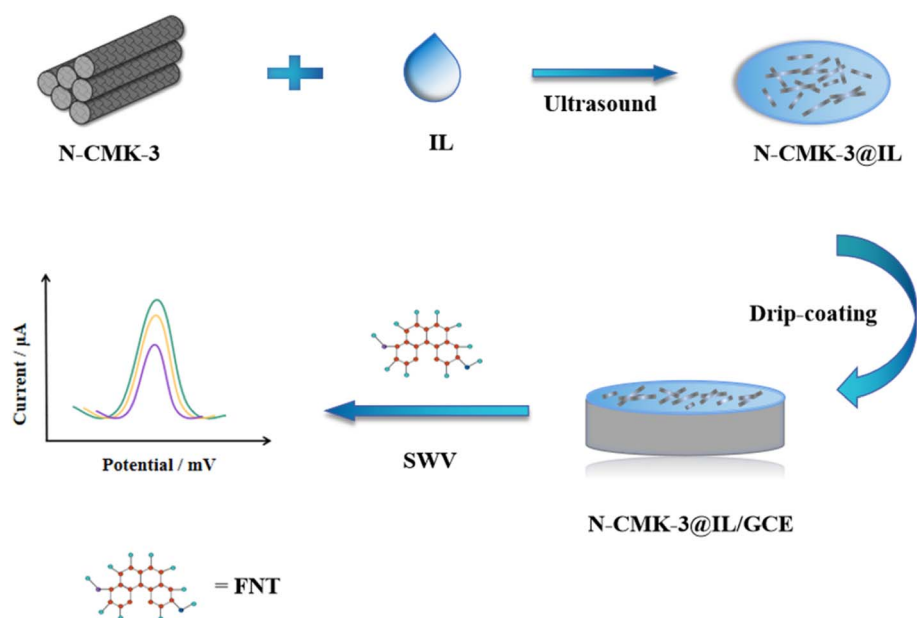
2.3. Electrode preparation

Nitrogen-doped mesoporous carbon@hydroxyl-functionalized ionic liquid composites (N-CMK-3@IL) were obtained by dispersing ultrasonically appropriate N-CMK-3 into the ionic liquid ([HOEtMlm]BF$_4$) solution for 30 min. The bare glassy carbon electrode (GCE) was polished into mirror surface with 0.3, and 0.05 μm alumina powder, and then cleaned by ultrasonic with 95% ethanol and ultrapure water, respectively. Finally, the glassy carbon electrode was dried by nitrogen. The nitrogen-doped mesoporous carbon@hydroxyl-functionalized ionic liquid composites modified glassy carbon electrode (N-CMK-3@IL/GCE) was prepared by dropping 7.0 μL N-CMK-3@IL composites onto glassy carbon electrode and dried under an infrared lamp.

For comparison, GCE and ionic liquid modified GCE (IL/GCE) were constructed in the similar procedure. The bare GCE was polished with alumina powder, and dried after ultrasonic cleaning. Then, 7.0 μL ionic liquid solution was applied to the GCE surface and dried in the infrared lamp. The obtained electrode was denoted as IL/GCE.

2.4. Analytical procedure

Cyclic voltammetry (CV) and electrochemical impedance spectroscopy (EIS) were utilized to investigate the electrochemical

Scheme 1 The preparation procedure of N-CMK-3@IL/GCE and electrochemical sensing process of FNT.

properties of the prepared sensors in 0.1 M KCl and 5 mM $K_3[Fe(CN)_6]/K_4[Fe(CN)_6]$ solution. The electrochemical behavior of FNT was studied by square wave voltammetry (SWV) in the range of −1.2 to −0.3 V with the accumulation time of 60 s. Scheme 1 shows the fabrication procedure of N-CMK-3@IL/GCE and the electrochemical sensing process of FNT.

3.   Results and discussion

3.1.   Surface morphologies and structural characterization

The surface morphologies of different modified electrodes were studied by scanning electron microscopy (SEM). As shown in Fig. 1a, bare GCE exhibited a smooth surface. On the surface of N-CMK-3/GCE (exhibited in Fig. 1b), N-CMK-3 was scattered in clusters. Fig. 1c displayed that N-CMK-3 was uniformly distributed and wrapped in ionic liquid on the surface of N-CMK-3@IL/GCE (shown in Fig. 1c) due to the high viscosity of the ionic liquid.

XPS analysis plays a significant role in characterizing functional groups on the surface of the composite materials. Fig. 2 records the XPS spectra of N-CMK-3@IL composites. As shown in Fig. 2A, N-CMK-3@IL composites contained C 1s, N 1s, O 1s, F 1s and N 1s transitions. It could be acquired by Elemental Analyzer that the amount of N in the composites was 11.07%. According to the C1s spectrum (exhibited in Fig. 2B), four deconvolution peaks could be observed at about 284.5 eV (C–C/C=C), 285.4 eV (C–N), 286.2 eV (C–O), and 288.6 eV (O–C=O), respectively. The formation of C–N verified the N atoms were doped into the N-CMK-3. As observed in Fig. 1c, the N 1s spectrum was fitted with two peaks at about 399.5 eV (pyrrolic-N) and 401.5 eV (graphitic-N), individually. The N-CMK-3@IL composites were beneficial for facilitating the electrochemical properties.

3.2.   CV and EIS characterization

Fig. 3 shows CVs of different electrodes in 0.1 M KCl and 5 mM $[Fe(CN)_6]^{3-/4-}$ solution. A pair of small redox peaks with the peak potential difference (ΔE_p) of 140 mV can be observed on GCE (curve a). When the ionic liquid was modified on the surface of GCE (IL/GCE, curve b), the response current of the sensor was increased and the ΔE_p was reduced to 104 mV. The results exhibited that IL/GCE owned better electrochemical properties compared with GCE. The peak current on N-CMK-3@IL composites modified electrode (curve c) further increased with the ΔE_p of 100 mV. There are several possible explanations for this result. On the one hand, N-CMK-3@IL composites have larger specific surface areas and can provide more electroactive sites. On the other hand, the composites can promote electron transfer rate between the analyte and the modified electrode.
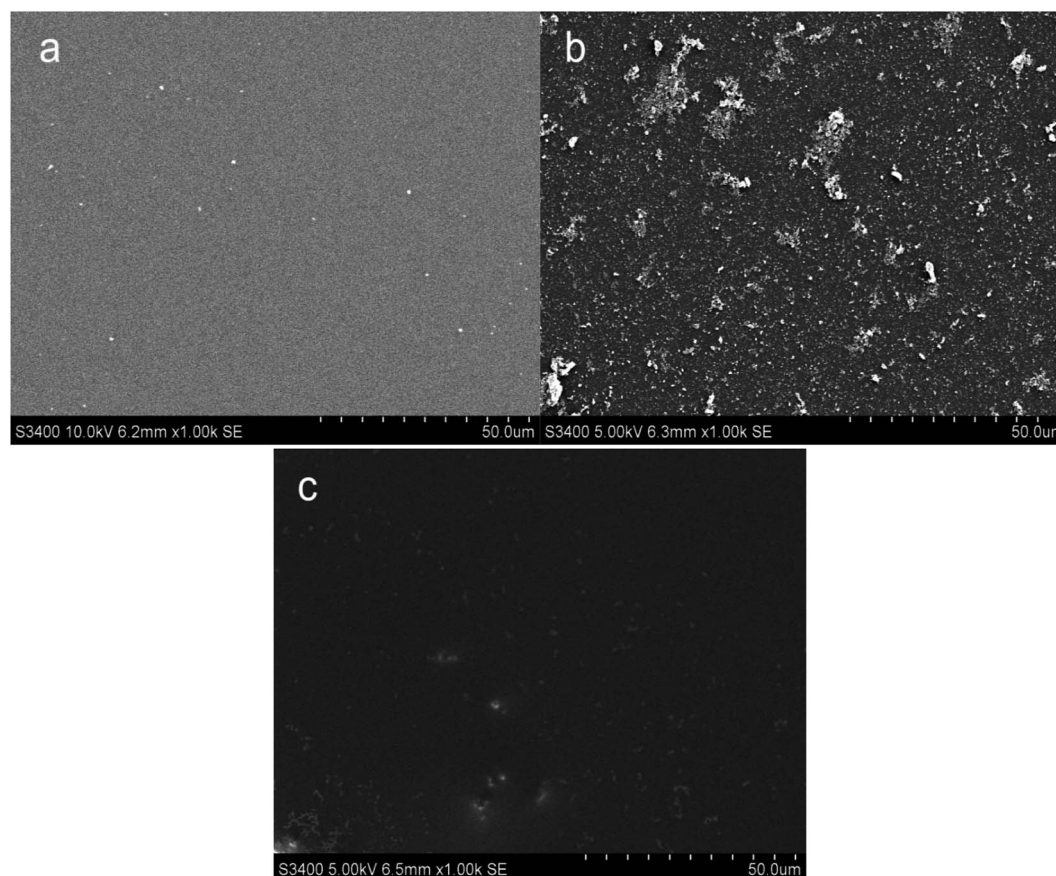

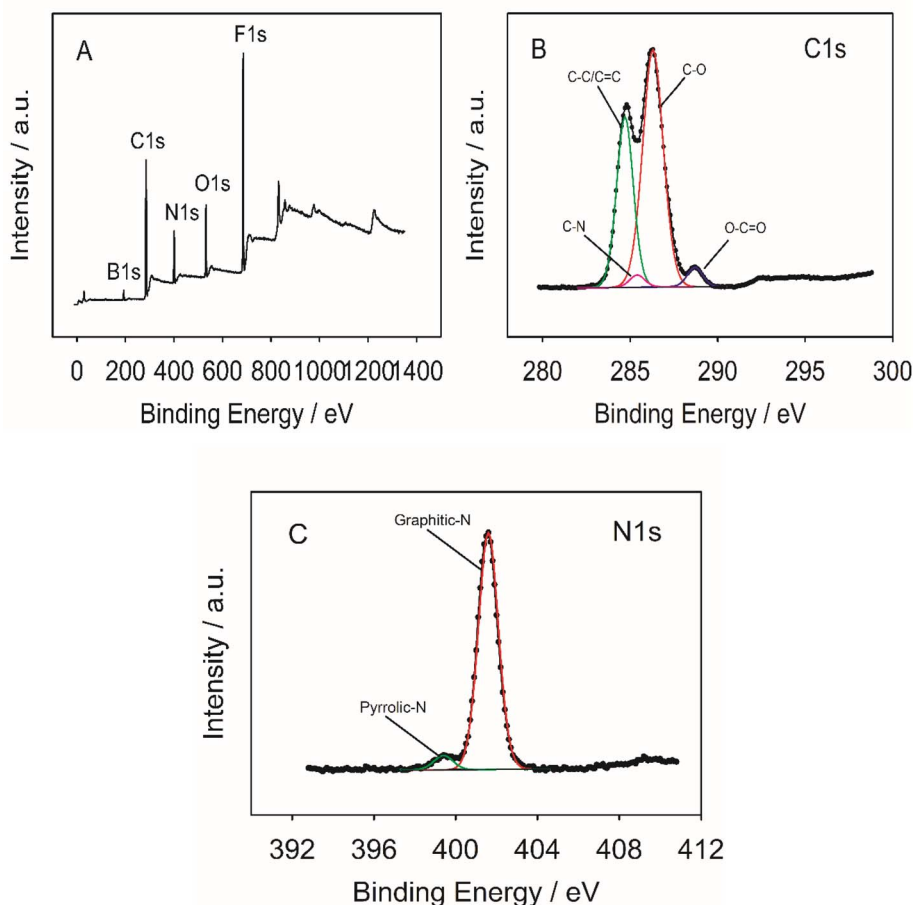Fig. 1   SEM images of (a) GCE, (b) N-CMK-3/GCE, (c) N-CMK-3@IL/GCE.

© 2023 The Author(s). Published by the Royal Society of Chemistry

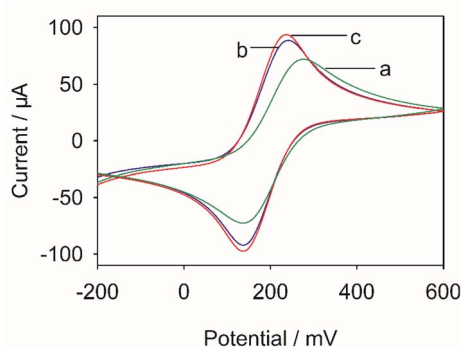**Fig. 2** XPS spectra of N–CMK-3@IL composites. (A) General spectrum (B) C 1s spectrum (C) N 1s spectrum.

Fig. 3 CVs of (a) GCE, (b) IL/GCE, (c) N–CMK-3@IL/GCE in 0.1 M KCl and 5 mM $[Fe(CN)_6]^{3-/4-}$ solution.

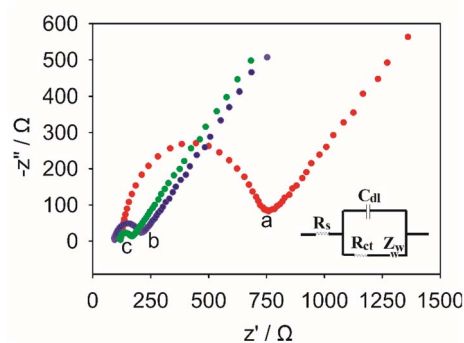**Fig. 4** EIS of (a) GCE, (b) IL/GCE, (c) N–CMK-3@IL/GCE in 0.1 M KCl and 5 mM $[Fe(CN)_6]^{3-/4-}$ solution.

Electrochemical impedance spectroscopy (EIS) was further employed to study the interfacial charge transfer properties. In EIS, the semicircle part in the high-frequency region represents the charge transfer resistance (R_{ct}). The larger the semicircle, the greater the R_{ct} value. Fig. 4 exhibits the Nyquist plots of the different modified electrodes. As shown in the figure, the bare GCE displayed the highest resistance (curve a).

However, after the GCE was modified with functional ionic liquid, the R_{ct} value of the modified electrode decreased significantly due to the excellent conductivity of ionic liquid. Compared with IL/GCE, the R^{ct} value of N–CMK-3@IL/GCE were further reduced. This could be attributed to the synergistic effect of N–CMK-3@IL composites in enhancing the conductivity of the sensor.
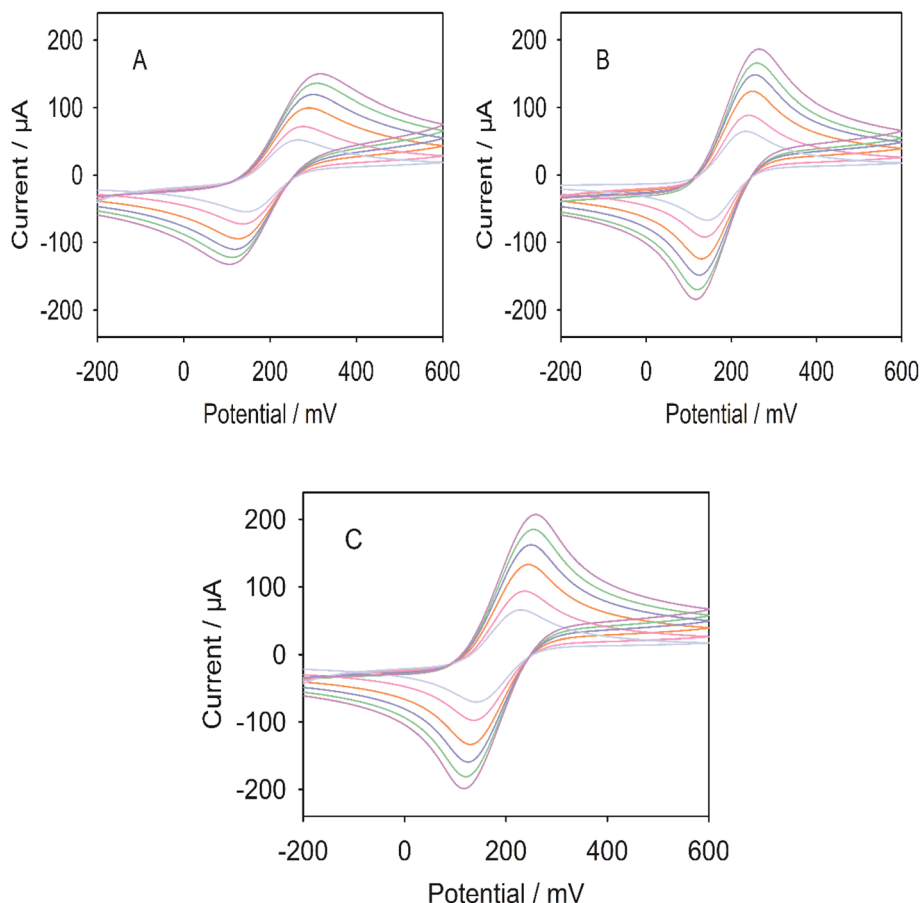
Fig. 5 CVs of (A) GCE, (B) IL/GCE, (C) N-CMK-3@IL/GCE in 0.1 M KCl and 5 mM [Fe(CN)$_6$]$^{3-/4-}$ solution with different scan rates (from inner to outer: 25, 50, 100, 150, 200, 250 mV s^{-1}).

3.3. Surface area study

As shown in Fig. 5, the effective surface area of different modified electrodes was studied in $K_3[Fe(CN)_6]/K_4[Fe(CN)_6]$ solution. According to the Randles–Sevcik equation,[19] the relationship between peak current (I_{pa}) and scan rate (ν) is as follows:

$$I_{pa} = (2.69 \times 10^5) n^{3/2} A C_0 D_R^{1/2} \nu^{1/2} \qquad (1)$$

where I_{pa} corresponds to the anode peak current; n and A represent the number of electron transfer ($n = 1$) and the electroactive surface area (cm^2), respectively; C_0 is the concentration of $K_3[Fe(CN)_6]$; D_R and ν are diffusion coefficient (7.6 × 10^{-6} cm^2 s^{-1}) and scan rate (V s^{-1}), respectively. Based on the slope of I_{pa} vs. $\nu^{1/2}$, the effective surface areas of GCE, IL/GCE, and N-CMK-3@IL/GCE were calculated to be 0.092 cm^2, 0.146 cm^2, and 0.172 cm^2, respectively. This result exhibited that N-CMK-3@IL/GCE presented larger specific surface area, which could provide more active binding sites for FNT.

3.4. Electrochemical behavior of FNT

Fig. 6 exhibits the SWVs of 20 ng mL^{-1} FNT at different modified electrodes. There was a small reduction peak of FNT on

GCE (Curve a). Compared to GCE, the current on IL/GCE (Curve b) increased obviously. The phenomenon indicated that the hydroxyl-functionalized ionic liquid was successfully modified on the GCE and effectively promoted electron transfer rate. Besides, the peak current of FNT further increased on N-CMK-3@IL/GCE (curve c), indicating that N-CMK-3@IL composites could improve the conductivity of the sensor and increase the adsorption capacity for FNT.
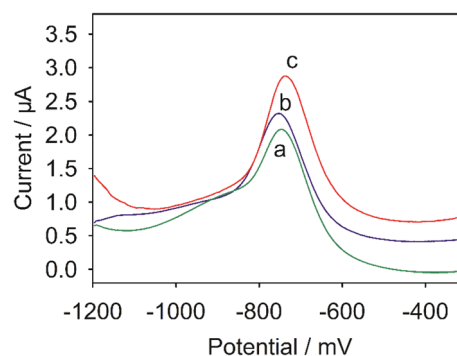

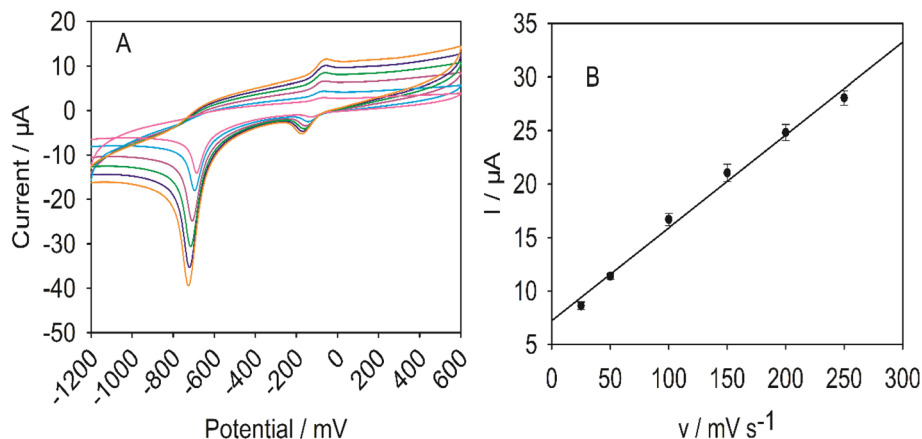**Fig. 6** SWVs of 20 ng mL^{-1} FNT at (a) GCE, (b) IL/GCE, (c) N-CMK-3@IL/GCE in 0.1 M pH 7.0 PBS.

Fig. 7 (A) CVs of 20 ng mL^{-1} FNT on N–CMK-3@IL/GCE with different scan rates (from inner to outer: 25, 50, 100, 150, 200, 250 mV s^{-1}). (B) The relationship between peak current and scan rate.

3.5. Effect of scan rate

The effect of scan rate on FNT response was investigated by CV. Fig. 7 shows the CVs of 20 ng mL^{-1} FNT on N–CMK-3@IL/GCE in the scan rate range of 25 to 250 mV s^{-1}. It can be observed that a pair of REDOX peaks and a reduction peak appeared in the reaction process, which is consistent with previous reports.[2] The possible reaction mechanism of FNT was exhibited in Scheme S1.† The irreversible reduction peak was attributed to reduction of the nitro group to the corresponding hydroxyl-amine group (reaction 1), and the reversible peaks were ascribed to the redox of nitroso-compound and hydroxylamine (reaction 2). The peak current increased with the scan rate, and their relationship conformed to the following equation: I (μA) = 0.0868 v (mV s^{-1}) + 7.2317 (r^2 = 0.9908), indicating that the reaction of fenitrothion on N–CMK-3@IL/GCE was an adsorption-controlled electrochemical process.

3.6. Optimization of experimental factors

3.6.1. Effect of pH value. The effect of supporting electrolytes with different pH values on FNT response was investigated in 0.1 M PBS. As exhibited in Fig. 8A, the current of FNT first

increased and then decreased in the range of pH 4.0–9.0, and reached its maximum at pH 7.0. This phenomenon could be ascribed to the decreasing proton concentration in the buffer which was necessary for the reduction of the nitro-group of FNT. Consequently, 0.1 M pH 7.0 PBS was selected for the subsequent experiments.

According to Fig. 8B, the peak potential of FNT shifted negatively as the pH value increased, showing a good linear relationship: E(V) = −0.0373 pH − 0.4698 (r^2 = 0.9949) with the slope was −37.3 mV pH^{-1}, which was consistent with the previous report.[20]

3.6.2. Effect of composites composition. As exhibited in Fig. 9, the influence of IL concentration on sensor performance was discussed. When the IL concentration increased from 1% to 5%, the peak current obviously increased. However, the further increase of IL concentration (from 5% to 10%) lead to the decrease of the peak current. A possible explanation for this might be that an appropriate amount of IL can effectively facilitate the electron transfer rate. In contrast, excess IL would increase the background current, resulting in a decrease of the FNT response. Therefore, 5% of IL concentration was chosen for the subsequent experiments.
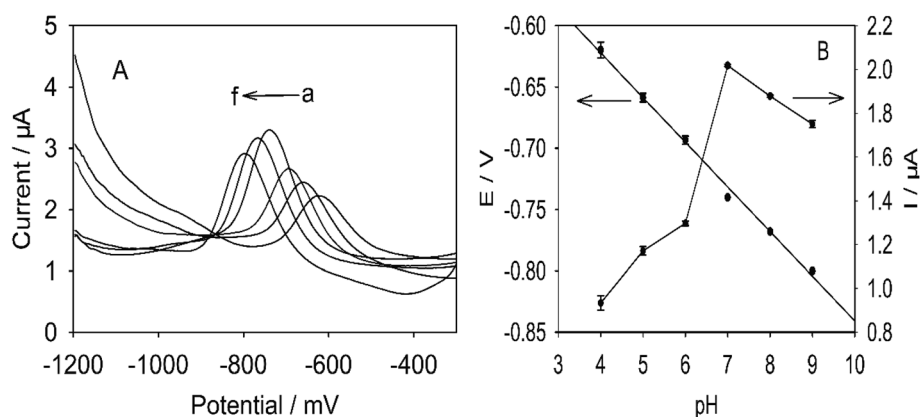

Fig. 8 (A) SWVs of 20 ng mL^{-1} FNT on N–CMK-3@IL/GCE in different pH solutions (from a to f: pH from 4.0 to 9.0). (B) Effect of pH value on the peak current and peak potential of FNT.
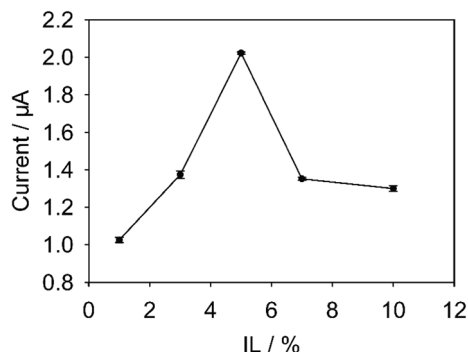
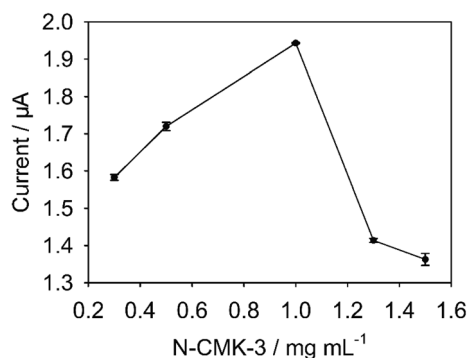**Fig. 9** Effect of IL concentration in composites on the current signal of 20 ng mL^{-1} FNT.

Fig. 12 Effect of the accumulation time on the current signal of 20 ng mL^{-1} FNT.

3.6.3. Effect of accumulation potential and time. Fig. 11 displays the response current of FNT at different accumulation potential. When the accumulation potential was applied, the maximum current of FNT was observed at −0.5 V. However, the larger current was obtained at open circuit potential (OCP). Thus, the enrichment of FNT would be carried on under open circuit potential. Fig. 12 explores the relationship between accumulation time and response current of FNT. The result exhibited that the accumulation of FNT on N-CMK-3@IL/GCE approached saturation at 60 s, and the longer accumulation time caused the decreased current. Therefore, 60 s was the optimal adsorption time of FNT.

Fig. 10 Effect of N-CMK-3 content in composites on the current signal of 20 ng mL^{-1} FNT.

The effect of N-CMK-3 content (from 0.3 to 1.5 mg mL^{-1}) on FNT current was represented in Fig. 10. The result suggested that the maximum peak current of FNT occurred at 1 mg mL^{-1} N-CMK-3. This phenomenon can be explained by the following reasons: The N-CMK-3 with pore structure could provide large specific surface areas, and the doping nitrogen atoms could offer more active centers. However, too much N-CMK-3 also lead to large background current. Therefore, 1 mg mL^{-1} of N-CMK-3@IL composite was utilized for the preparation of the sensor.
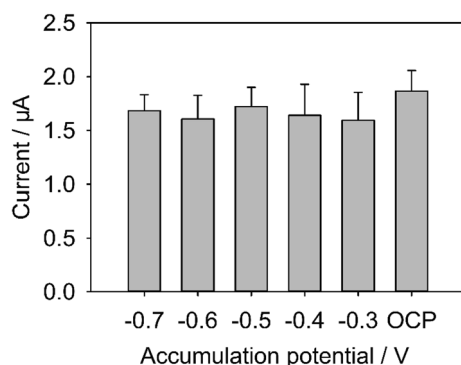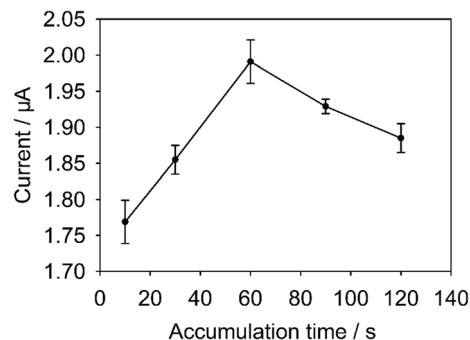
3.7. Determination of FNT

The SWVs of FNT with different concentrations on N-CMK-3@IL/GCE were shown in Fig. 13. The peak current of FNT varied linearly with its concentration in the range of 0.5–100 ng mL^{-1}. The regression equation was: $I (\mu A) = 0.0321 c$ (ng mL^{-1}) $+ 0.7521$ ($r^2 = 0.9947$), with the detection limit of 0.1 ng mL^{-1} (S/N = 3). Table 1 compares the analytical parameters of different FNT sensors.[21–24] The N-CMK-3@IL/GCE in this work exhibited excellent electrochemical performance with lower detection limit and wider linear range.

3.8. Reproducibility, stability, and specificity

The reproducibility of N-CMK-3@IL/GCE was discussed in 0.1 M pH 7.0 PBS containing 20 ng mL^{-1}. The FNT response current on six electrodes prepared in the same process showed good reproducibility with a relative standard deviation (RSD) of 1.11%. After one-month storage at 4 °C, the response signal of FNT maintained 93.62% of the initial current, exhibiting excellent stability of the sensor.

The anti-interference ability of N-CMK-3@IL/GCE was also explored. As shown in Table S1,† the interference experiments exhibited that 1000-fold concentration of Ca^{2+}, Cd^{2+}, Fe^{2+}, K$^+$, Zn^{2+}, Cl$^-$, NO$_3^-$, SO$_4^{2-}$, 100-fold concentration of dopamine (DA), ascorbic acid (AA), uric acid (UA), glucose, 10-fold concentration of p-nitrophenol and nitrobenzene have little effects on the response signals of FNT, suggesting the good selectivity of the sensor.
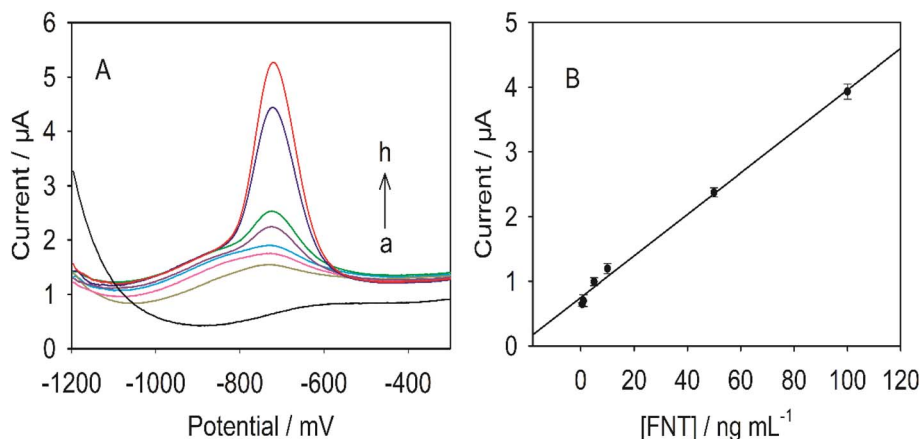

Fig. 11 Effect of the accumulation potential on the current signal of 20 ng mL^{-1} FNT.

Fig. 13 (A) SWVs for various concentrations of FNT (from a to h: 0, 0.1, 0.5, 1, 5, 10, 50, 100 ng mL^{-1} FNT). (B) The calibration graph of FNT.

Table 1 Comparison of the analytical performance of the different modified electrodes for determination of FNT

Modified electrode	Method	Linear range (ng mL^{-1})	Limit of detection (ng mL^{-1})	Reference
CeO$_2$[a]/rGO[b]/GCE[c]	SWV	5.54–554.4	0.832	21
RGO/DPA[d]/PGE[e]	SWV	27.72–529.51	0.97	22
Nano-TiO$_2$/Nafion/GCE	DPV	55.45–1.109 × 10^3	24.95	23
ZrO$_2$[f]/RGO/MoS$_2$-Au[g]/AuE[h]	SWV	4.99–5.99 × 10^3	2.2	24
N-CMK-3@IL/GCE	SWV	0.5–100	0.1	This work

[a] CeO$_2$: cerium(IV) oxide. [b] rGO: reduced graphene oxide. [c] GCE: glassy carbon electrode. [d] DPA: poly(E)-1-(4-((4-(phenylamino)phenyl)diazenyl)phenyl)ethanone. [e] PGE: pencil graphite electrode. [f] ZrO$_2$: zirconia nanoparticles. [g] MoS$_2$-Au: molybdenum sulfide-Au. [h] AuE: gold electrode.

Table 2 Determination of FNT on N-CMK-3@IL/GCE in vegetable samples ($n = 3^a$)

	Cabbage	Lettuce	Greens
Added/ng mL^{-1}	5.00	5.00	5.00
Detected/ng mL^{-1}	4.95	5.24	4.84
Recovery/%	99.1	104.9	96.9
RSD/%	1.99	2.42	0.87

[a] Three different measurements were made for each sample.

3.9. Sample analysis

The feasibility of N-CMK-3@IL/GCE in practice application was investigated by the standard addition method. The lettuce, cabbage, and greens were purchased from the local market. The samples were first ground, then filtered, and the supernatant was extracted. Before measurement the obtained supernatant was diluted 50 times with 0.1 M pH 7.0 PBS. The detection results are shown in Table 2. The recoveries varied in the range of 96.9–104.9%, proving that the sensor based on N-CMK-3@IL/GCE has good application prospects.

4. Conclusion

In summary, a non-enzymatic FNT sensor was successfully prepared based on nitrogen-doped mesoporous carbon@hydroxyl-functionalized ionic liquid composites. Due to the unique porous structure of nitrogen-doped mesoporous carbon and the superior electrical conductivity of the functionalized ionic liquid, the sensor showed good adsorption and catalytic performance toward FNT. The sensor exhibited low detection limit, good stability and selectivity. The proposed method could be successfully applied to detect FNT in vegetable samples.

Author contributions

Xinsheng Liu: writing—original draft preparation, and visualization; Yutong Li: software, investigation and data curation; Wenli Qiao: methodology, software, validation; Mengjun Chang: software, investigation, and visualization; Yonghong Li: writing—review & editing and supervision.

Conflicts of interest

The authors declare that they have no competing interests.

Acknowledgements

References

1 R. R. Shi, W. T. Zou, Z. L. Zhao, G. Q. Wang, M. Guo, S. Y. Ai, Q. Zhou, F. C. Zhao and Z. Y. Yang, Development of a sensitive phage-mimotope and horseradish peroxidase based electrochemical immunosensor for detection of O,O-dimethyl organophosphorus pesticides, *Biosens. Bioelectron.*, 2022, **218**, 114748.

2 A. Özcan, D. Topçuoğulları and A. A. Özcan, Fenitrothion sensing with reduced graphene oxide decorated fumed silica nanocomposite modified glassy carbon electrode, *Sens. Actuators, B*, 2019, **284**, 179–185.

3 S. M. H. Sereshti, Three-dimensional graphene aerogel-supported iron oxide nanoparticles as an efficient adsorbent for magnetic solid phase extraction of organophosphorus pesticide residues in fruit juices followed by gas chromatographic determination, *J. Chromatogr. A*, 2016, **1443**, 43–53.

4 A. M. Filho, F. N. D. Santos and P. A. D. P. Pereira, Development, validation and application of a methodology based on solid-phase micro extraction followed by gas chromatography coupled to mass spectrometry (SPME/GC-MS) for the determination of pesticide residues in mangoes, *Talanta*, 2010, **81**, 346–354.

5 C. C. Yu, D. Y. Hao, Q. Chu, T. Wang, S. N. Liu, T. Lan, F. H. Wang and C. P. Pan, A one adsorbent QuEChERS method coupled with LC-MS/MS for simultaneous determination of 10 organophosphorus pesticide residues in tea, *Food Chem.*, 2020, **321**, 126657.

6 M. Bhattu, M. Verma and D. Kathuria, Recent advancements in the detection of organophosphate pesticides: a review, *Anal. Methods*, 2021, **13**, 4390–4428.

7 G. D. Liu and Y. H. Lin, Electrochemical sensor for organophosphate pesticides and nerve agents using zirconia nanoparticles as selective sorbents, *Anal. Chem.*, 2005, **77**, 5894–5901.

8 J. H. Wu, Q. T. Yang, Q. Li, H. Y. Li and F. Li, Two-dimensional MnO₂ nanozyme-mediated homogeneous electrochemical detection of organophosphate pesticides without the interference of H₂O₂ and Color, *Anal. Chem.*, 2021, **93**, 4084–4091.

9 K. Jangid, R. P. Sahu, S. Sakib, I. Zhitomirsky and I. K. Puri, Surface-Modified Metal Oxides for Ultrasensitive Electrochemical Detection of Organophosphates, Heavy Metals, and Nutrients, *ACS Appl. Nano Mater.*, 2022, **5**, 17183–17193.

10 L. S. Porto, L. F. Ferreira, W. T. P. dos Santos and A. C. Pereira, Determination of organophosphorus compounds in water and food samples using a non-enzymatic electrochemical sensor based on silver nanoparticles and carbon nanotubes nanocomposite coupled with batch injection analysis, *Talanta*, 2022, **246**, 123477.

11 M. Ganesan, R. K. Devi, A. H. Liao, K. Y. Lee, G. Gopalakrishnan and H. C. Chuang, 3D-flower-like porous neodymium molybdate nanostructure for trace level detection of organophosphorus pesticide in food samples, *Food Chem.*, 2022, **396**, 133722.

12 H. Ehzari, M. Safari, M. Samimi, M. Shamsipur and M. B. Gholivand, A highly sensitive electrochemical biosensor for chlorpyrifos pesticide detection using the adsorbent nanomatrix contain the human serum albumin and the Pd:CdTe quantum dots, *Microchem. J.*, 2022, **179**, 107424.

13 D. X. Nie, P. Li, D. Zhang, T. S. Zhou, Y. Liang and G. Y. Shi, Simultaneous determination of nitroaromatic compounds in water using capillary electrophoresis with amperometric detection on an electrode modified with a mesoporous nano-structured carbon material, *Electrophoresis*, 2010, **31**, 2981–2988.

14 H. Dai, Y. Y. Lin, G. F. Xu, L. S. Gong, C. P. Yang, X. L. Ma and G. N. Chen, Cathodic electrochemiluminescence of luminol using polyaniline/ordered mesoporous carbon (CMK-3) hybrid modified electrode for signal amplification, *Electrochim. Acta*, 2012, **78**, 508–514.

15 H. W. Wang, Y. Q. Liu, G. X. Hu, Y. J. Ye, L. L. Pan, P. J. Zhu and S. Yao, Ultrasensitive electrochemical sensor for determination of trace carbadox with ordered mesoporous carbon/GCE, *J. Electroanal. Chem.*, 2020, **857**, 113736.

16 S. H. Zhou, H. B. Xu, J. Y. Liu, Y. J. Wei, X. H. Ma, Z. M. Han and H. L. Chen, Simplified synthesis of N-doped carbon nanotube arrayed mesoporous carbon for electrochemical detection of amitrole, *Chem. Phys.*, 2021, **542**, 111074.

17 H. Bagheri, A. Afkhami, H. Khoshsafar, M. Rezaei, S. J. Sabounchei and M. Sarlakifar, Simultaneous electrochemical sensing of thallium, lead and mercury using a novel ionic liquid/graphene modified electrode, *Anal. Chim. Acta*, 2015, **870**, 56–66.

18 H. J. Gao, T. T. Kan, S. Y. Zhao, Y. X. Qian, X. Y. Cheng, W. L. Wu, X. D. Wang and L. Q. Zheng, Removal of anionic azo dyes from aqueous solution by functional ionic liquid cross-linked polymer, *J. Hazard. Mater.*, 2013, **261**, 83–90.

19 Y. Li, Y. T. Li, Y. Wang, G. D. Ma, X. S. Liu, Y. H. Li and J. Soar, Application of zeolitic imidazolate frameworks (ZIF-8)/ionic liquid composites modified nano-carbon paste electrode as sensor for electroanalytical sensing of 1-hydroxypyrene, *Microchem. J.*, 2020, **159**, 105433.

20 M. Govindasamy, U. Rajji, S. M. Chen, S. Kumaravel, T. W. Chen, F. M. A. Al-Hemaid, M. A. Ali and M. S. Elshikh, Detection of Pesticide Residues (Fenitrothion) in Fruit samples based on Niobium Carbide@Molybdenum Nanocomposite: An Electrocatalytic Approach, *Anal. Chim. Acta*, 2018, **1030**, 52–60.

21 A. A. Ensafi, R. Noroozi, N. Zandi-Atashbar and B. Rezaei, Cerium(IV) oxide decorated on reduced graphene oxide, a selective and sensitive electrochemical sensor for fenitrothion determination, *Sens. Actuators, B*, 2017, **245**, 980–987.

22 O. Surucu, G. Bolat and S. Abaci, Electrochemical behavior and voltammetric detection of fenitrothion based on a pencil graphite electrode modified with reduced graphene oxide (RGO)/poly(*E*)-1-(4-((4-(phenylamino)

phenyl)diazenyl)phenyl)ethanone (DPA) composite film, *Talanta*, 2017, **168**, 113–120.

23 A. Kumaravel and M. Chandrasekaran, A biocompatible nano TiO_2/Nafion composite modified glassy carbon electrode for the detection of fenitrothion, *J. Electroanal. Chem.*, 2011, **650**, 163–170.

24 P. P. Qi, J. Wang, X. Wang, X. Y. Wang, Z. W. Wang, H. Xu, S. S. Di, Q. Wang and X. Q. Wang, Sensitive determination of fenitrothion in water samples based on an electrochemical sensor layered reduced graphene oxide, molybdenum sulfide (MoS_2)-Au and zirconia films, *Electrochim. Acta*, 2018, **292**, 667–675.